J Appl Electrochem (2009) 39:2275–2284
DOI 10.1007/s10800-008-9762-5

ORIGINAL PAPER

# Electrochemical study of self-assembled cysteine monolayers on polycrystalline gold electrodes and functionalization with microperoxidase MP-11

**Ignasi Sirés · Marina Delucchi · Marco Panizza · Rico Ricotti · Giacomo Cerisola**

Received: 1 October 2008 / Accepted: 16 December 2008 / Published online: 8 January 2009


**Abstract** Self-assembled monolayers of cysteine (CYST) have been constructed on polycrystalline gold (polyAu) electrode at different immersion times ($t_{immer}$) in order to characterize them by cyclic voltammetry and electrochemical impedance spectroscopy (EIS). Oxidative desorption experiments allowed the calculation of the surface coverage, whereas reductive desorption informed about the binding of CYST to different gold domains. Desorption products showed different diffusion ability. The maximum coverage was already achieved at short $t_{immer}$, although progressive reordering of CYST molecules led to a relevant decrease of the defects at long time, as ascertained by EIS. Functionalization of polyAu-CYST electrodes with the enzyme microperoxidase MP-11 performed by following two different binding methods showed that the enzymatically catalyzed reduction of $H_2O_2$ is enhanced when the –COOH residues of the MP-11 undecapeptide chain are firstly activated and then linked to the $–NH_2$ functional groups of the non-activated CYST layer formed on the polyAu surface.

**Keywords** Self-assembled monolayers · Cysteine · Microperoxidase · $H_2O_2$ reduction · Biosensors · Biofuel cells

I. Sirés (✉) · M. Delucchi · M. Panizza · R. Ricotti · G. Cerisola
Dipartimento di Ingegneria Chimica e di Processo "G.B. Bonino", Università degli Studi di Genova, P.le J.F. Kennedy 1, 16129 Genoa, Italy
e-mail: isires@catalonia.net

## 1 Introduction

Molecular self-assembly is a popular method for electrode modification and functionalization, due to its simplicity, versatility, reproducibility, high level of molecular ordering and ability to permit control over the packing density [1, 2]. Moreover, it offers the possibility of applying a wide variety of characterization techniques and incorporating multiple molecular components enabling the interface to fulfill a variety of functions. The term *self-assembly* is commonly used but it can cause confusion. Generally, it may be defined as the spontaneous formation of complex hierarchical structures from pre-designed building blocks [3].

Many recent works have focused on self-assembled monolayers (SAMs) of organic alkanethiols, disulfides and sulfides, which become strongly chemisorbed with high order on various metal surfaces such as gold, due to the significant affinity of the sulfur atoms for the gold surface. Construction of SAMs has been mostly carried out on single gold crystals, mainly Au(111) substrates. Reports on the fate of SAMs constructed onto polycrystalline gold substrates are much more scarce, due to its surface roughness that complicates the interpretation of some surface processes, although such roughness can be preferable to smoother surfaces for some applications, such as sensing.

Recent advances and applications of SAMs have been extensively reviewed by several authors [4, 5]. SAMs constitute a versatile tool for the preparation of bio-surfaces, particularly appealing for the future development of biosensors and biofuel cells [2, 6]. Electrochemistry of metalloproteins and pure enzymes is a subject of great interest, but electron transfer becomes extremely slow at an electrode surface, thereby hindering detection of signals. Modification of electrode surfaces paved the way to solve

this problem. Among the various enzymes available, microperoxidases are especially interesting because they display peroxidase activity, that is, they catalytically reduce $H_2O_2$ to water [7]. $H_2O_2$ is a strong oxidant, yet its electrochemical reduction proceeds with a high overpotential. The bioelectrocatalyzed reduction of $H_2O_2$ to water has been achieved by using various peroxidases. Microperoxidase MP-11 is an α-helical undecapeptide connected via two thioether bonds to an Fe(III)-protoporphyrin IX heme site. It is obtained by controlled hydrolytic digestion of horse heart cytochrome *c* and it corresponds to the active site microenvironment of the cytochrome. MP-11 presents several advantages compared to its original protein, such as small size, high stability and direct electron transfer [8]. It is well known that no electrochemical activity of MP-11 is detected at a bare Au electrode [9]. Lötzbeyer and co-workers [10–12] were pioneers in the immobilization of MP-11 onto gold surface. They investigated the characteristics of MP-11 by means of cyclic voltammetry. Direct, reversible and fast electron transfer between the active heme site and the electrode surface involving a non-diffusing $Fe^{3+}/Fe^{2+}$ redox couple was shown, being the redox potential $E^0 = -398 \pm 5$ mV/SCE [10, 13, 14], as also confirmed by Jiang et al. when using 3-mercaptopropionic acid to bind MP-11 [15]. In the past, the efficient reduction of $H_2O_2$ by MP-11-functionalized gold electrodes has been mainly ascertained by using a cystamine-modified gold surface.

On the other hand, the very promising surface modifier cysteine (CYST) has received much less attention, despite being very useful for the preparation of bioactive surfaces. CYST is an aminoacid (i.e., a bifunctional aminothiol) that can be bound to MP-11 through its $–NH_2$ or –COOH group, thus offering the possibility of developing different methodologies for the growth of SAMs on gold. However, scarce studies on its use for MP-11 deposition have been reported [9]. In fact, papers on CYST SAMs on gold basically deal with their electrochemical characterization [16–24]. The adsorption or formation of a film of CYST on gold has been studied by various groups and is attributed to the following process [17]:

$$RSH \rightarrow RS_{ads} + H^+ + e^- \quad (1)$$

where R is the amino acid functionality.

This process provides a monolayer of CYST across the gold surface and has been characterized, revealing that CYST is adsorbed as a thiolate, like other organosulfur compounds. It is stated that the sulfur headgroup sits at the bridge site between two surface Au atoms, and the $S–C_\beta$ bond is tilted by 57° [19, 23].

Indeed, CYST is an interesting system to study, so in this work we have formed CYST SAMs onto a polycrystalline gold surface upon immersion of the electrode into an aqueous solution containing the aminoacid. The films have been characterized by cyclic voltammetry (CV) and electrochemical impedance spectroscopy (EIS), following a comparative study between the oxidative and reductive desorption processes that allowed determining the surface coverage. The particularities of the SAM behavior have been assessed by CV in phosphate buffer and KOH media, and EIS measurements were done to know if long immersion time of gold into the CYST solution leads to the best conditions for modification due to the formation of compact SAMs with a small amount of defects and pinholes. Finally, the modified gold surface was functionalized with MP-11 to prepare a bioelectrode able to carry out the reduction of $H_2O_2$, for its potential use in the fields of biosensors and biofuel cells.

## 2 Experimental

### 2.1 Reagents and solutions

L-cysteine ((R)-2-amino-3-mercaptopropionic acid or CYST, see structure in Fig. 1) hydrochloride monohydrate (≥99%) from Fluka was used to prepare 100 mM aqueous CYST solutions and form the thiol SAMs on gold electrode. Since CYST is air sensitive and readily oxidized, the solution must be prepared daily. 1 M HEPES (4-(2-hydroxyethyl)-1-piperazineethanesulfonic acid) sodium salt buffer solution of pH 7.5 as well as 1-ethyl-3-(3-dimethylaminopropyl)-carbodiimide hydrochloride (EDC, ≥98%) used as coupling agent or cross-linker to activate the carboxylic residues at the protein or the thiol molecules were also purchased from Fluka. Microperoxidase MP-11 sodium salt (~90%) was from Sigma. $K_3Fe(CN)_6$ was used as redox probe in some cyclovoltammetric measurements.

0.1 M phosphate buffer saline (PBS) medium of pH 6.9, prepared from $Na_2HPO_4 \cdot 12H_2O$ and $KH_2PO_4$, was used for most of the experiments because is the usual physiological medium for biological studies.

$H_2O_2$ used to assess the reduction ability of MP-11-functionalized electrodes was from Fluka and the concentration of the different standard solutions tested was determined from titration with a standard solution of $KMnO_4$ and light absorption of the titanic-hydrogen peroxide colored complex at $\lambda = 408$ nm [25].

All chemicals were analytical or reagent grade and were used as received. All solutions were prepared with double-distilled (pure) water.

### 2.2 Electrochemical measurements

The voltammetric and electrochemical impedance measurements were performed by using a PGSTAT30 potentiostat/galvanostat from AUTOLAB (EcoChemie,

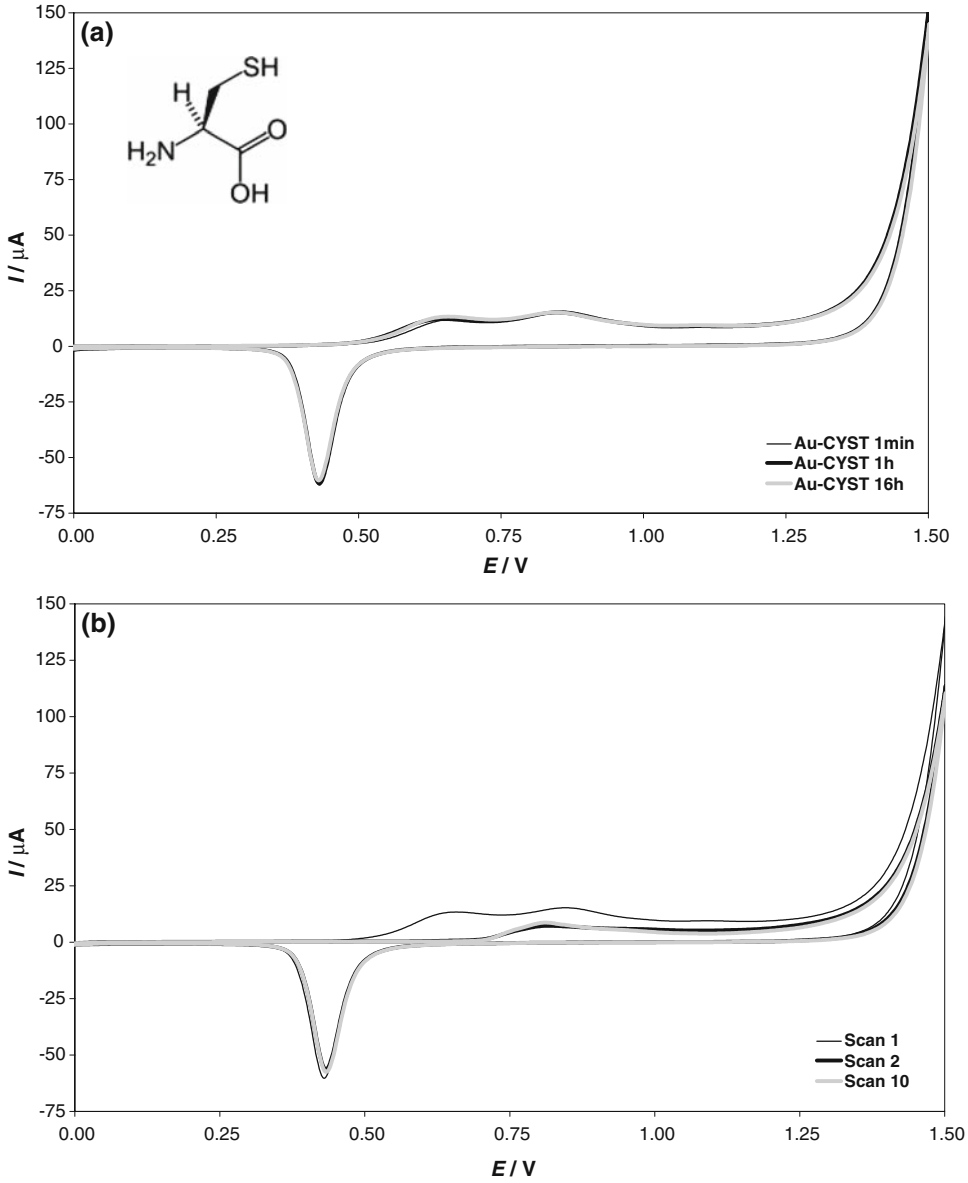


**Fig. 1** Oxidative desorption of cysteine (CYST) from polyAu-CYST SAMs in 0.1 mM phosphate buffer solution (PBS, pH 6.9) in the potential range between −0.045 and +1.5 V vs. Ag|AgCl|KCl (sat.). Scan rate = 50 mV $s^{-1}$ (starting at 0 V and sweeping towards positive potentials); room temperature. **a** First scans of cyclic voltammograms corresponding to different immersion times ($t_{immer}$ = 1 min, 1 h and 16 h) of the polyAu electrode in 100 mM CYST solution are compared. The chemical structure of CYST is also shown. **b** Scans 1, 2 and 10 with the electrode at $t_{immer}$ = 16 h

Netherlands) interfaced with a personal computer controlled by General Purpose Electrochemical System GPES 4.6 and FRA softwares. Both electrode preparation and electrochemical measurements were performed at room temperature (23 ± 2 °C).

A polycrystalline Au electrode tip (polyAu, i.e., polycrystalline gold rotating disk electrode sealed in a PTFE jacket, Metrohm 6.1204.020, Switzerland) was used as working electrode, being its exposed geometrical surface area 0.07 $cm^2$ ($\phi$ = 3.04 mm). The roughness factor (r.f.) was estimated after 30 scans in 0.5 M $H_2SO_4$ in the potential region between 0.045 and 1.545 V vs. Ag|AgCl|KCl (sat.) (corresponding to the typically suggested sweep between 0 and 1.5 V/SCE, according to Sawyer et al. [26]). A value of r.f. = 1.4 was estimated for the polyAu electrode as calculated from the charge consumed during the removal of the gold oxide monolayer, taking (390 ± 10) μC $cm^{-2}$ as the reference oxide reduction charge for a polyAu electrode [27, 28]. Accordingly, the real area of the polyAu electrode used in this work was calculated to be 0.099 $cm^2$.

All experiments were carried out in a conventional three-electrode glass cell, using a Ag|AgCl|KCl (sat.) and a Pt wire as reference and counter electrodes, respectively. All reported potentials in this paper are referenced to the Ag|AgCl|KCl (sat.) electrode. The electrochemical cell was placed in a Faraday cage to eliminate any environmental stray effect. In all cases, 100 mL solutions were used. Deaerating nitrogen gas was bubbled through the solutions for 20 min prior to measurement, and a nitrogen blanket was kept during the recording of the voltammograms or the impedances.

All cyclic voltammetries were performed at 50 mV $s^{-1}$. Except reductive desorption studies performed in 0.5 M KOH, all electrochemical measurements were made in 0.1 M PBS medium of pH 6.9. For the EIS measurements a sine wave with 5 mV amplitude was applied in order to obtain a linear response of the system, and the impedances were measured for 40 frequencies logarithmically distributed between 10 kHz and 50 mHz. The EIS data were fitted using appropriate equivalent electronic circuits via FRA software, and model parameters such as interfacial charge-transfer resistance ($R_{ct}$) and the capacitance ($C$) were extracted in 0.1 M PBS medium.

For SAM characterization, measurements of the bare and modified electrodes with different SAMs were always recorded. All measurements were carried out at least twice in order to verify all the observations made.

### 2.3 Electrode preparation and modification

The cleaning of the gold electrode is a step of critical importance for SAM formation and it should be accomplished systematically. Before SAM preparation, an accurate cleaning process of the polyAu surface must be done. Firstly, the electrode is polished with $Al_2O_3$ slurry 0.3 μm (Metrohm, Switzerland) on microcloth pads to a mirror finish, and then it is rinsed with pure water. In a second step, any remaining polishing powder is removed from the surface by ultrasonic treatment. With this aim, the electrode is ultrasonicated in absolute ethanol and in pure water for 10 min each. Finally, residual contaminants on bare gold can be removed electrochemically by cycling the potential between 0.045 and 1.545 V in 0.5 M $H_2SO_4$ at 100 mV $s^{-1}$ until a stable characteristic voltammogram is obtained (typically 30 scans, when a CV curve with invariant gold oxide formation and reduction peaks is reached). The cleanliness can be ascertained by comparison of the *I–E* curve with that of the clean polyAu reported by Flinkea et al. [29] and Brett et al. [30].

Next, to prepare a well-assembled monolayer, the freshly pretreated electrode is immediately dipped (i.e., immersion method) in the solution of the organosulfur ligand during a certain immersion time ($t_{immer}$). The polyAu-CYST electrode is ready for measurements or further modification after being rinsed with pure water to remove physically adsorbed molecules, and then dried under nitrogen atmosphere. The literature shows a point of some controversy concerning the stability and rate of oxidation of the Au-SAMs in laboratory environments. In the present study, only for long $t_{immer}$ as well as for storage the electrodes were kept at 4 °C under nitrogen atmosphere in order to minimize possible oxidation.

To prepare the polyAu-CYST-MP-11 electrode we have compared two modification methods:

*Method 1*—Activation of the –COOH residues of the CYST: a Au-CYST electrode prepared for 16 h as explained above was immersed into a solution containing 10 mM EDC and 10 mM HEPES buffer and maintained at 4 °C for 2 h. After rinsing it properly, the electrode exhibiting the activated carboxylic residues of CYST was immersed into a solution containing 0.3 mM MP-11 and 10 mM HEPES buffer and maintained at 4 °C for 3 h.

*Method 2*—Activation of the –COOH residues of the MP-11 (i.e., the carboxylic groups associated with the protoporphyrin ligand or those ones found in the oligopeptide chain): a Au-CYST electrode prepared for 16 h as explained above was immersed into a solution containing 0.3 mM MP-11, 10 mM EDC and 10 mM HEPES buffer and maintained at 4 °C for 3 h.

The polyAu-CYST-MP-11 electrode is thoroughly rinsed with pure water and dried under nitrogen atmosphere prior to measurements.

The reaction mechanism of the EDC coupling of a carboxylic acid and an amine group to form an amide is explained elsewhere [31]. At the end of each specific study and prior to preparing a recently used electrode for a new modification, the complete destruction of the layers onto it was ascertained by recording cyclic voltammograms in the potential region between −1.0 and +1.5 V (the scan direction was positive, and the scans were initiated at 0 V) in 0.1 M PBS medium at 50 mV $s^{-1}$ until a voltammogram analogous to the one obtained for bare gold was obtained (typically 10 scans).

## 3 Results and discussion

### 3.1 Oxidative and reductive desorption of cysteine

Porter and co-workers [32] found that *n*-alkanethiols adsorbed on gold surfaces can be both oxidatively and reductively desorbed. The exact potential at which SAMs oxidatively or reductively desorbs is influenced by the actual alkanethiol (i.e., chain length and head group repulsion), as this determines the integrity of the SAM.

Firstly, the oxidative desorption of CYST from polyAu-CYST electrode was studied in 0.1 mM PBS medium in the potential range between −0.045 and +1.5 V (starting at 0 V and sweeping towards positive potentials). The first scans of cyclic voltammograms corresponding to different immersion times ($t_{immer}$ = 1 min, 1 h and 16 h) of the polyAu electrode in 100 mM CYST solution are represented in Fig. 1a. All curves are almost analogous and they present some significant features: (i) a positive current is appreciated from about +470 mV, with a first peak appearing at +665 mV and a second peak at +850 mV, and afterwards the current increases up to its maximum

value at +1.5 V; (ii) during the sweep towards negative potentials, a peak corresponding to gold oxide reduction is observed at +430 mV. The fact that no changes are observed with increasing $t_{immer}$ suggests that CYST SAMs are spontaneously and suddenly formed, reaching the maximum surface coverage ($\Gamma_{CYST}$) very quickly. Consecutive scans were recorded for the polyAu-CYST electrode at $t_{immer} = 16$ h to calculate $\Gamma_{CYST}$. Figure 1b summarizes scans 1, 2 and 10. It can be seen that curves for scans 2 and 10 are equal. A positive current is observed from about +700 mV, with a sole peak at +810 mV. As in the first scan, current rises up to +1.5 V, and a peak corresponding to gold oxide reduction is observed at +430 mV. In fact, the cyclovoltammogram corresponding to a bare polyAu electrode under the same conditions (not shown) matches perfectly with that of the second scan, what is a clear evidence of the complete oxidative desorption of CYST during the first scan. Whereas the adsorption of CYST on the polyAu surface proceeds via reaction (1), as commented above, leading to the formation of an organothiolate film, the oxidative desorption of previously adsorbed CYST is believed to occur according to reaction (2) [17]:

$$RS_{ads} + 3H_2O \rightarrow RSO_3^- + 6H^+ + 5e^-. \quad (2)$$

The product, cysteinesulfonic acid (or cysteic acid), is desorbed from the gold surface and easily diffuses into the bulk solution as it is formed. This prevents from re-adsorption and allows considering the process as an irreversible oxidative desorption of CYST. Reaction (2) occurs concomitantly with the formation of gold surface oxide, as deduced from the presence of the two peaks in the first scan (+665 and +850 mV). This is also supported by the finding that the charge corresponding to the gold oxide reduction peak at +430 mV is practically identical to that obtained with the bare polyAu electrode [33].

With all these considerations in mind, differences in charge values between the first and second scan of Fig. 1b can be attributed to the charge required for the oxidation of the adsorbed CYST layer. Experimentally, we have integrated both voltammograms between +470 mV and 1.5 V, obtaining 234 and 115 μC for the first and second scan, respectively. This yields a charge of 119 μC entirely corresponding to desorption of CYST. Using this charge value and taking $n = 5$ e$^-$ from reaction (2), application of Faraday's law allows the calculation of the amount of CYST adsorbed on the polyAu surface, resulting $\Gamma_{CYST} = 2.5$ nmol cm$^{-2}$. This result agrees very well with the value of 2.7 nmol cm$^{-2}$ reported by Arrigan and Le Bihan [17] and 2.3 nmol cm$^{-2}$ reported by Fawcett et al. [16].

Some cyclovoltammograms obtained between −1.0 and +1.5 V (also starting at 0 V and sweeping towards positive potentials) were identical to the previous ones, confirming that CYST is completely desorbed in the gold oxide formation region during the first positive scan.

Secondly, the reductive desorption of CYST from polyAu-CYST electrode was studied in deaerated 0.5 mM KOH solution, cycling the potential between 0 and −1.3 V (starting at 0 V).

It is been widely shown that the charge required for the reductive desorption in alkaline medium is a useful tool for characterizing SAMs. For example, it has been used to measure the surface coverage by adsorbed thiols, disulfides or sulfides, which resist against desorption over a wide potential range but at very negative potentials and in strongly alkaline electrolytes are desorbed quantitatively. Figure 2a shows the first scans of cyclic voltammograms corresponding to bare polyAu and to $t_{immer} = 1$ min, 1 h and 16 h in 100 mM CYST solution. In contrast to oxidative desorption, differences were found at different $t_{immer}$. Three characteristic reduction peaks (A, B and C in Fig. 2a) were found: peak A at −730 mV only appear at 16 h, whereas peaks B and C at −1020 and −1120 mV, respectively, are already present from short $t_{immer}$. The existence of these three peaks has been discussed by several authors, and it can be concluded that the polyAu electrode surface is mainly composed of three low-index crystallographic orientations, i.e., Au(111), Au(110) and Au(100) [20–22]. According to the potential needed for the reductive desorption of CYST from single crystalline gold domains, peaks A, B and C correspond to Au(111), Au(100) and Au(110), respectively [22]. There is a competitive chemisorption of CYST on the different surface domains of the polyAu, with the understanding that the thiol molecules exhibit different binding strengths towards each surface domain leading to the appearance of the multiple reductive desorption peaks. At $t_{immer} = 1$ min and 1 h, only strongly bound CYST molecules are adsorbed on polyAu, so just peaks B and C are found during desorption experiments. At 16 h, also loosely bound CYST is adsorbed, thus appearing peak A in Fig. 2a. In conclusion, CYST molecules adsorb preferentially and consecutively at the Au(110), Au(100) and then at the Au(111) surface domains, which exhibits the lowest affinity for thiol chemisorption and consequently the most positive potential. For the calculation of $\Gamma_{CYST}$, it must be taken into account that the electrochemical reaction for thiol reductive desorption on gold accomplishes the following one-electron stoichiometric relationship [34]:

$$R\text{-}S\text{-}Au + e^- \leftrightarrow Au + RS^-. \quad (3)$$

Desorption charges were obtained from the first CVs after correction for the related backgrounds obtained from average of base currents on the sides of the related peaks. Note that a significant increase in the base current, which is

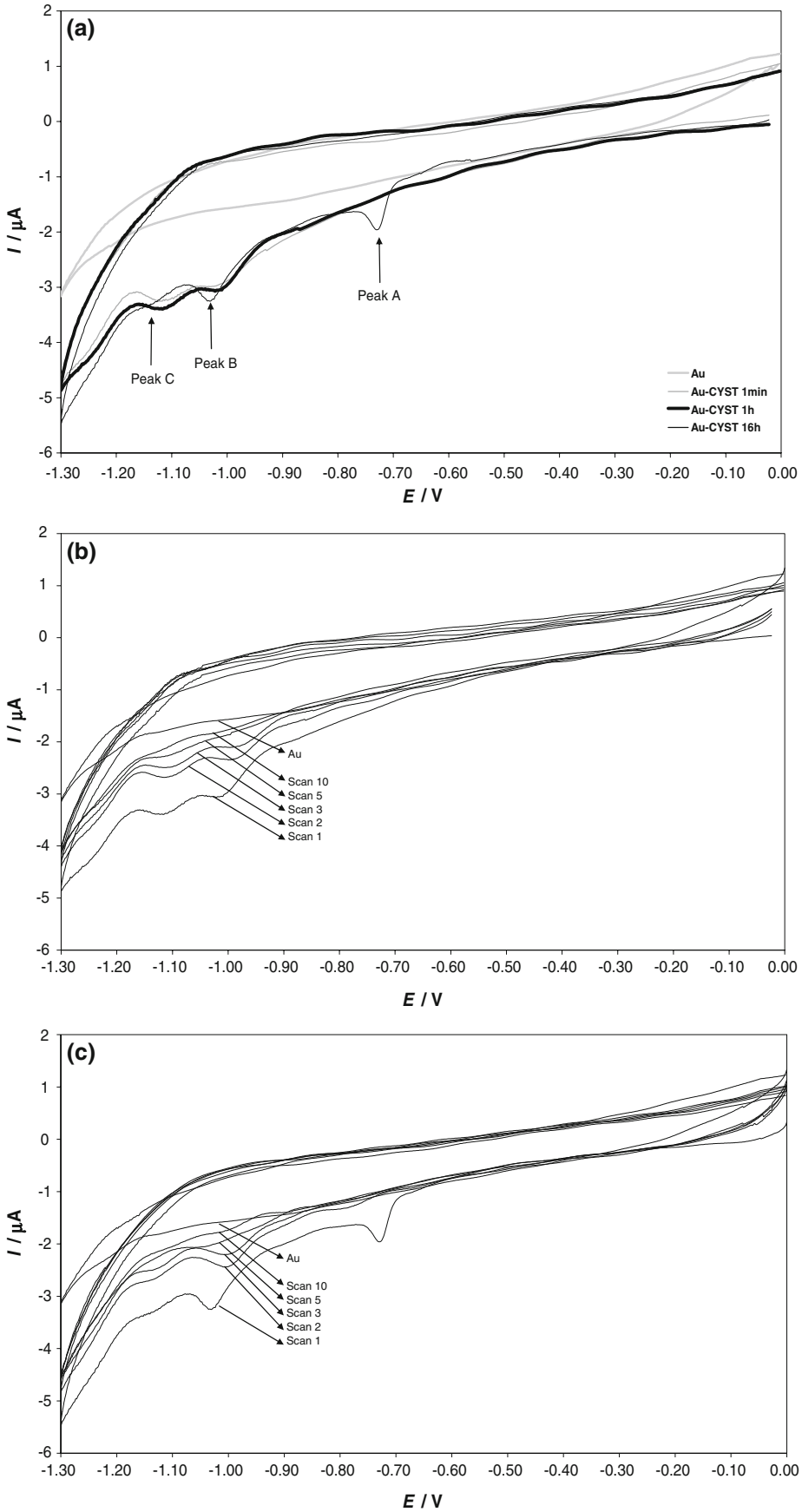


**Fig. 2** Reductive desorption of CYST from polyAu-CYST SAMs in 0.5 mM KOH solution in the potential range between 0 and −1.3 V vs. Ag|AgCl|KCl (sat.). Scan rate = 50 mV $s^{-1}$ (starting at 0 V); room temperature. **a** First scans of cyclic voltammograms corresponding to bare polyAu and to $t_{immer}$ = 1 min, 1 h and 16 h are compared. **b** Scans 1, 2, 3, 5 and 10 with the electrode at $t_{immer}$ = 1 h and cyclovoltammogram corresponding to bare polyAu. **c** Scans 1, 2, 3, 5 and 10 with the electrode at $t_{immer}$ = 16 h and cyclovoltammogram corresponding to bare polyAu

proportional to the double-layer capacitance, is observed after the reduction peak, confirming the thiol desorption as a thiolate [35]. Interestingly, the total $Q$ (including all the gold domains observed) is very similar for all $t_{immer}$, as found during oxidative desorption in PBS medium, just varying the preferential domains covered in each case. It suggests that the maximum $\Gamma_{CYST}$ is already achieved at short time, although the calculated value of 0.5 nmol $cm^{-2}$ differs from the coverage of $(1.5 \pm 0.2)$ nmol $cm^{-2}$ reported in literature [21] and even from the value determined above. This is due to the difficult measurement of the reduction charge in comparison to the easier integration in the oxidative desorption experiments.

Figure 2b shows consecutive scans 1–10 for the polyAu-CYST electrode at $t_{immer} = 1$ h and cyclovoltammogram corresponding to bare polyAu. Continuous potential cycling leads to complete desorption of the CYST SAM from the electrode surface after 10 scans. The peak potential ($E_p$) of peaks B and C reveals the shift to more positive potential values as the coverage decreases (i.e., as the number of cycles increases). The changing intermolecular interactions between adsorbed CYST molecules (bond stretching, bending angles, steric hindrance, electrostatic and van der Waals interactions) can account for such shift: in more compact monolayers such as those ones existing in the initial scan, the spacing between CYST molecules is shorter than in the more sparsely SAMs formed as cycling progresses, so that both the chain–chain interactions and the electrostatic interactions are higher. Intermolecular interactions are weaker at higher number of scans, resulting in the shift of $E_p$ to more positive values (i.e., easier desorption).

Figure 2c is similar to Fig. 2b, although it presents the consecutive scans for $t_{immer} = 16$ h. The positive shift of $E_p$ is observed again, and it is worth noting that peak A disappears during the first scan, confirming that the Au(111) domain exhibits the lowest affinity for CYST adsorption.

Figure 2b and c seem to indicate that reductive desorption of CYST is a gradual process, contrary to what observed for its oxidative desorption, because a progressive disappearance of the reduction peaks is found. However, we believe that thiolate formed from CYST reduction shown in reaction (3) is completely desorbed during the first scan but, since its diffusion towards the bulk solution is not as favored as in the case of cysteic acid, it is able to be partially re-adsorbed, thus exhibiting a kind of gradual desorption.

Results of oxidative and reductive CYST desorption discussed up to now do not reflect significant differences when increasing $t_{immer}$.

### 3.2 Integrity of the polyAu-CYST SAMs

The insulating properties of prepared SAMs have been evaluated by comparing two electrochemical methods. Firstly, in order to study the electron-transfer reaction we have plotted in Fig. 3 the positive sweeps of the cyclic voltammograms corresponding to bare polyAu and to polyAu-CYST electrode at $t_{immer} = 5$ min and 1 h in 0.1 mM PBS medium containing 5 mM $K_3Fe(CN)_6$ as redox probe in the potential range between −0.055 and +0.445 V (starting at −0.055 V). Reversible voltammograms were always obtained (the peak at negative potential is not shown), indicating that the electron-transfer reaction is diffusion controlled. As shown, the oxidation peak for the redox process of the probe is found at +262 mV. No remarkable differences can be appreciated in the current

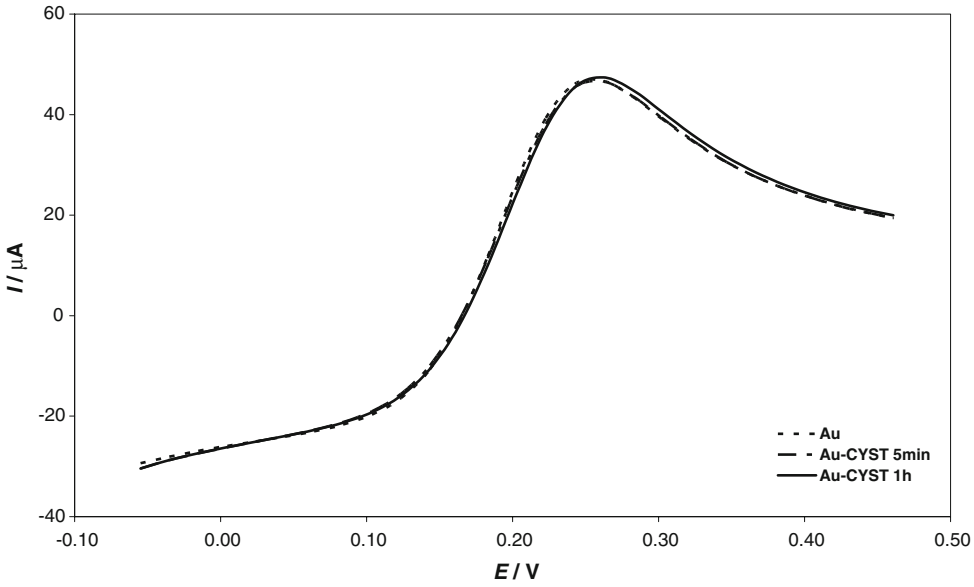


**Fig. 3** Positive sweeps of the cyclic voltammograms corresponding to bare polyAu and to polyAu-CYST SAMs at $t_{immer} = 5$ min and 1 h in 0.1 mM PBS medium containing 5 mM $K_3Fe(CN)_6$ in the potential range between −0.055 and +0.445 V vs. Ag|AgCl|KCl (sat.). Scan rate = 50 mV $s^{-1}$; room temperature

values, obtaining between 46 and 48 μC with or without the CYST layer. This means that the ions have easy access through the pinholes and pores present in the CYST SAM.

The decrease in the peak current when considering the oxidation/reduction of a redox couple can be related to the fractional coverage of the monolayer ($\theta^{CV}$) [36]:

$$\theta^{CV} = 1 - \frac{I_p^{SAM}}{I_p^{Au}}. \quad (4)$$

However, in the present case it is not a very useful parameter, since the presence of many defects in the SAM at these immersion times leads to a wrong determination of the coverage. It has been shown a porous open monolayer structure amenable to solvent, electrolyte and probe molecule permeation, so CYST film does not block the surface, unlike the case with long alkyl chain SAMs [17].

Next, a more sensitive method like EIS was used. This is a powerful tool to determine the kinetic parameters, the insulating properties and the density of the SAM. Figure 4 shows the Nyquist plots corresponding to bare polyAu and to polyAu-CYST SAMs at $t_{immer}$ = 0.5 min, 5 min and 1 h in 0.1 mM PBS medium. The equivalent circuit to fit the experimental data is also presented. It can be modeled as a constant phase element (CPE) in parallel with the charge-transfer resistance $R_{ct}$, which are then connected to the series resistance $R_s$ [37]. A CPE is used instead of a pure capacitor to compensate for the non-ideal capacitive response of the interface, arisen from inhomogeneties [38].

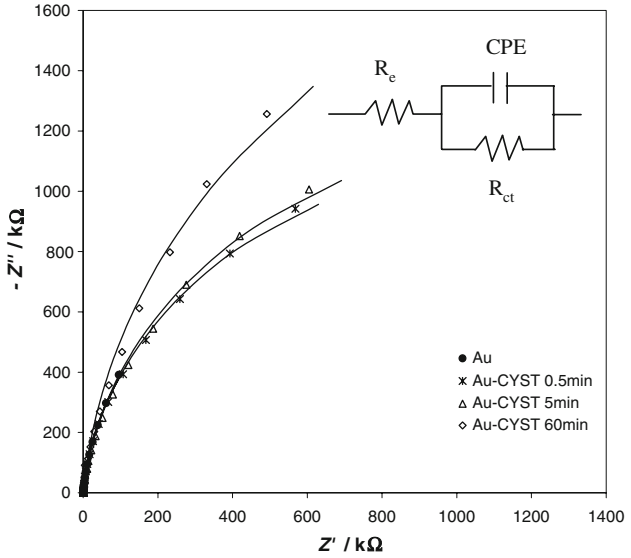


**Fig. 4** Electrochemical assessment of the SAMs integrity by EIS. Nyquist plots corresponding to bare polyAu and to polyAu-CYST SAMs at $t_{immer}$ = 0.5 min, 5 min and 1 h in 0.1 mM PBS medium. Begin frequency = 10 kHz; end frequency = 50 mHz; amplitude = 5 mV; number of frequencies = 40 (logarithmic distribution); room temperature. The equivalent circuit used to fit the experimental values is also shown

In order to reduce the uncertainties caused by different gold substrates we repeated each test three times and the values of fitted circuit elements are the mean of those obtained in both fittings. In the Nyquist plot, the diameter of the semicircle at high frequencies corresponds to the magnitude of $R_{ct}$. The impedance plot of the bare polyAu electrode exhibits a much smaller semicircular diameter ($R_{ct}$ = 1.00 kW) than those observed for all polyAu-CYST experiments. Also, it can be seen that the semicircular diameter enlarged with increasing $t_{immer}$, implying a higher electron-transfer resistance, possibly due to the increased thickness and compactness of the CYST layer. The $R_{ct}$ value increases from 2.75 kW at 0.5 min to 4.05 kW at 60 min. But, it must be noted that the value at 5 min is 2.80 kW, which is very close to that at 0.5 min. So, the first fast kinetic step (i.e., the quick adsorption of CYST molecules, shown from the clear increase of $R_{ct}$ from polyAu to polyAu-CYST at 0.5 min) is easily observable, and afterwards several adsorption/ordering steps occur, until SAM gets its final state at long time [39]. Such slow reorganization of the CYST molecules with increasing $t_{immer}$ allows enhancing the integrity of the SAM by decreasing the amount of defects and pinholes [30, 40]. Thus, longer $t_{immer}$ leads to greater packing and inhibition of the electron transference. Regarding the capacitance values, a progressive decrease was found, as expected from the thickening of the CYST layer. We obtained 7.00, 1.95 and 1.70 μF for bare polyAu, 0.5 and 60 min, respectively. In conclusion, the impedance data offer a better understanding of the phenomena that take place, demonstrating that long $t_{immer}$ favors the stabilization and correct ordering of the CYST molecules, presumably leading to the enhanced modification with biomolecules.

### 3.3 Functionalization with MP-11 for $H_2O_2$ reduction

After the intense electrochemical characterization of the polyAu-CYST electrode, the cross-linker EDC was used to functionalize it by activating the –COOH groups of CYST or MP-11. Functionalization *methods 1* and *2* described above were compared. The selected biomolecule immobilization method interferes in the performance of the biosensors, such as sensitivity, selectivity and stability, so it must be carefully assessed [41]. The enzymatically catalyzed reduction of $H_2O_2$ was studied in 0.1 mM PBS medium containing different $H_2O_2$ concentrations in the range from 0.1 to 1 mM. In Fig. 5, the reduction current density ($j$) obtained with the functionalized polyAu-CYST-MP-11 electrode in a solution containing 1 mM $H_2O_2$ has been represented. At −100 mV, $j$-values of −0.60 and −0.76 μA cm$^{-2}$ were obtained with *method 1* (dotted line) and *2* (continuous line), meaning that better results are achieved when activating MP-11, because its –COOH

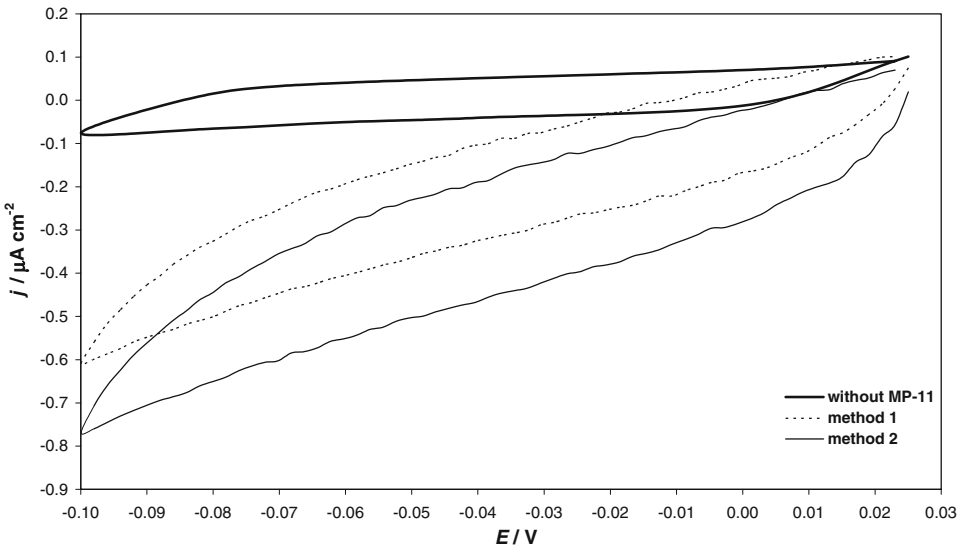


**Fig. 5** Reduction current density in the potential range between +25 and −100 mV vs. Ag|AgCl|KCl (sat.) with the functionalized polyAu-CYST-MP-11 electrode in 0.1 mM PBS medium containing 1 mM $H_2O_2$. Functionalization methods 1 (*dotted line*) and 2 (*plain continuous line*) described in the text are compared. The reference plot obtained with an unmodified polyAu-CYST in the same conditions is also shown (*bold continuous line*). Scan rate = 10 mV $s^{-1}$ (starting at +25 mV); room temperature

residues can be favorably linked to the $–NH_2$ group of CYST. Similarly, immobilization of horseradish peroxidase by using the $–NH_2$ terminal groups of the prepared SAMs provided the best results, associated to high sensitivity for $H_2O_2$ reduction with such biosensor [41].

As expected, a very low current density value was obtained with both electrodes in the absence of $H_2O_2$ (not shown). Also, the reduction current density obtained with 1 mM $H_2O_2$ by using a Au-CYST electrode prepared for 16 h without functionalization with MP-11 was very low, as depicted in the figure, thus demonstrating the efficacy of electrodes modified with MP-11. Moreover, an increasing $j$ was always found with increasing $H_2O_2$ concentration in the range from 0.1 to 1 mM, being observed a non-proportional dependence between $j$ and $[H_2O_2]$. Thus, $j$ increased from about $-0.10$ µA $cm^{-2}$ for 0.1 mM $H_2O_2$ to $-0.60$ µA $cm^{-2}$ in the case of *method 1*, whereas it changed from about $-0.15$ mA $cm^{-2}$ to $-0.76$ µA $cm^{-2}$ with *method 2*. An asymptotic increase was shown up to the maximum $j$ obtained at 1 mM $H_2O_2$, possibly indicating mass transfer limitations. To assess this phenomenon, the polyAu-CYST-MP-11 electrode was then used in the rotating mode. Higher $H_2O_2$ concentrations were used but no significant enhancement of $j$ was obtained, indicating saturation of the reduction ability of MP-11 or instability/degradation of the enzyme at too high $H_2O_2$ concentration.

Finally, some brief studies on the stability of the modified electrode where carried out: (i) the response loss after a high number of cycles for 3 h was followed to assess the behavior of the electrode under continuous use, and (ii) the variation of the reduction current density with 1 mM $H_2O_2$ was investigated to assess the temporal stability of the electrode kept at 4 °C during a whole week. In both cases, a progressive decay of the reduction signal was observed, being more significant in the former experiment, where the signal quickly decreased to half the value after 1 h. Further research is required to improve the stability of the MP-11-functionalized biocathode.

## 4 Conclusion

The electrochemical characterization of polyAu-CYST electrodes prepared after immersion in a 100 mM CYST aqueous solution at different $t_{immer}$ allows drawing up some conclusions concerning the formation, growth and integrity of the monolayers formed:

- The maximum surface coverage of $\Gamma_{CYST} = 2.5$ n-mol $cm^{-2}$, already achieved after $t_{immer} = 1$ min, is easily calculated by oxidative desorption in PBS medium and agrees well with reported values, whereas the existence of preferential gold domains for CYST binding is only observed by reductive desorption in 0.5 M KOH.
- Desorption products show different diffusion ability: oxidative desorption involves 5 $e^-$ and leads to the formation of cysteic acid that diffuses well, whereas reductive desorption involves 1 $e^-$ and yields thiolate that can be re-adsorbed onto the polyAu, thus mimicking a gradual desorption process.
- The best conditions for the formation of Au-CYST SAMs involve long $t_{immer}$ (16 h), because in spite of showing similar coverage, it is said to yield more ordered layers. The thickness and compactness of the CYST layers increases with time, as revealed by the rising charge-transfer resistance and the decreasing capacitance obtained by EIS.

Once the particularities of such modified electrodes have been clarified and aiming to explore their potential

application in the field of biofuel cells or biosensors, a biocathode was prepared by binding the enzyme MP-11 following two different methodologies. It has been demonstrated that the enzymatically catalyzed reduction of $H_2O_2$ is enhanced when activating the –COOH residues of the MP-11 to bind them to the $–NH_2$ groups of the non-activated CYST molecules, thus yielding a reduction current density of $-0.76$ μA $cm^{-2}$ at $-100$ mV.

**Acknowledgments** I.S. acknowledges the support from the members of the *Laboratorio di Elettrochimica, Corrosione e Protezione dei Materiali Metallici* of the *Università degli Studi di Genova* to draw up this paper.

## References

1. Russell Everett W, Fritsch-Faules I (1995) Anal Chim Acta 307:253–268
2. Ferretti S, Paynter S, Russell DA, Sapsford KE, Richardson DJ (2000) Trends Analyt Chem 19:530–540
3. Schreiber F (2004) J Phys Condens Matter 16:R881–R900
4. Gooding JJ, Mearns F, Yang W, Liu J (2003) Electroanalysis 15:81–96
5. Love JC, Estroff LA, Kriebel JK, Nuzzo RG, Whitesides GM (2005) Chem Rev 105:1103–1169
6. Bullen RA, Arnot TC, Lakeman JB, Walsh FC (2006) Biosens Bioelectron 21:2015–2045
7. Kadnikova EN, Kostić NM (2003) J Org Chem 68:2600–2608
8. Katz E, Shipway AN, Willner I (2003) In: Vielstich W, Gasteiger HA, Lamm A (eds) Handbook of fuel cells—fundamentals, technology and applications, vol 1, chap 21. Wiley, New York
9. Santucci R, Brunori M, Campanella L, Tranchida G (1992) Bioelectrochem Bioenerg 29:177–184
10. Lötzbeyer T, Schuhmann W, Katz E, Falter J, Schmidt H-L (1994) J Electroanal Chem 377:291–294
11. Lötzbeyer T, Schuhmann W, Schmidt H-L (1996) Sens Actuators B Chem 33:50–54
12. Kranz C, Lötzbeyer T, Schmidt H-L, Schuhmann W (1997) Biosens Bioelectron 12:257–266
13. Patolsky F, Gabriel T, Willner I (1999) J Electroanal Chem 479:69–73
14. Ruzgas T, Gaigalas A, Gorton L (1999) J Electroanal Chem 469:123–131
15. Jiang L, Glidle A, McNeil CJ, Cooper JM (1997) Biosens Bioelectron 12:1143–1155
16. Fawcett WR, Fedurco M, Kovácová Z, Borkowska Z (1994) Langmuir 10:912–919
17. Arrigan DWM, Le Bihan L (1999) Analyst 124:1645–1649
18. Shin T, Kim K-N, Lee C-W, Shin SK, Kang H (2003) J Phys Chem B 107:11674–11681
19. Di Felice R, Selloni A, Molinari E (2003) J Phys Chem B 107:1151–1156
20. Arihara K, Ariga T, Takashima N, Arihara K, Okajima T, Kitamura F, Tokuda K, Ohsaka T (2003) Phys Chem Chem Phys 5:3758–3761
21. El-Deab MS, Ohsaka T (2003) Electrochem Commun 5:214–219
22. El-Deab MS, Ohsaka T (2004) Electrochim Acta 49:2189–2194
23. Cavalleri O, Gonella G, Terreni S, Vignolo M, Floreano L, Morgante A, Canepa M, Rolandi R (2004) Phys Chem Chem Phys 6:4042–4046
24. Ivanov I, Vidakovic TR, Sundmacher K (2008) Electrochem Commun 10:1307–1310
25. Welcher FJ (1975) Standard methods of chemical analysis, vol 2, 6th edn. Krieger RE Publication Co, New York, p 1827, part B
26. Sawyer DT, Sobkowiak A, Roberts JL Jr (1995) Electrochemistry for chemists, 2nd edn. Wiley, New York
27. Trasatti S, Petrii OA (1991) Pure Appl Chem 63:711–734
28. Carvalhal RF, Freire RS, Kubota LT (2005) Electroanalysis 17:1251–1259
29. Finklea HO, Avery S, Lynch M, Furtsch T (1987) Langmuir 3:409–413
30. Brett CMA, Kresak S, Hianik T, Brett AMO (2003) Electroanalysis 15:557–565
31. Matemadombo F, Westbroek P, Nyokong T, Ozoemena K, De Clerck K, Kiekens P (2007) Electrochim Acta 52:2024–2031
32. Walczak MM, Popenoe DD, Deinhammer RS, Lamp BD, Chung C, Porter MD (1991) Langmuir 7:2687–2693
33. Wirde M, Gelius U, Nyholm L (1999) Langmuir 15:6370–6378
34. Kawaguchi T, Yasuda H, Shimazu K, Porter MD (2000) Langmuir 16:9830–9840
35. Imabayashi S-I, Iida M, Hobara D, Feng ZQ, Niki K, Kakiuchi T (1997) J Electroanal Chem 428:33–38
36. Campuzano S, Pedrero M, Montemayor C, Fatás E, Pingarrón JM (2006) J Electroanal Chem 586:112–121
37. Ding S-J, Chang B-W, Wu C-C, Lai M-F, Chang H-C (2005) Anal Chim Acta 554:43–51
38. Schweiss R, Werner C, Knoll W (2003) J Electroanal Chem 540:145–151
39. Shervedani RK, Hatefi-Mehrjardi A, Babadi MK (2007) Electrochim Acta 52:7051–7060
40. Ganesh V, Kumar Pal S, Kumar S, Lakshminarayanan V (2006) J Colloid Interf Sci 296:195–203
41. Mendes RK, Carvalhal RF, Kubota LT (2008) J Electroanal Chem 612:164–172